



HAL
open science

Experimental and Numerical study on Aerodynamics of Aerofoils at Low Reynolds Number Controlled by Off-Surface Micro-Vortex Generators

A. Larabi, Michael Pereira, Florent Ravelet, Tarik Azzam, T Ait-Ali, H. Oualli, Farid Bakir

► To cite this version:

A. Larabi, Michael Pereira, Florent Ravelet, Tarik Azzam, T Ait-Ali, et al.. Experimental and Numerical study on Aerodynamics of Aerofoils at Low Reynolds Number Controlled by Off-Surface Micro-Vortex Generators. Congrès Français de Mécanique, 2022, Nantes, France. hal-03755727

HAL Id: hal-03755727

<https://hal.science/hal-03755727>

Submitted on 22 Aug 2022

HAL is a multi-disciplinary open access archive for the deposit and dissemination of scientific research documents, whether they are published or not. The documents may come from teaching and research institutions in France or abroad, or from public or private research centers.

L'archive ouverte pluridisciplinaire **HAL**, est destinée au dépôt et à la diffusion de documents scientifiques de niveau recherche, publiés ou non, émanant des établissements d'enseignement et de recherche français ou étrangers, des laboratoires publics ou privés.

Experimental and Numerical study on Aerodynamics of Aerofoils at Low Reynolds Number Controlled by Off-Surface Micro-Vortex Generators

A. LARABI^a, M. PEREIRA^b, F. RAVELET^b, T. AZZAM^a, T.
AIT-ALI^a, H. OUALLI^a, F. BAKIR^b

a. Laboratoire de Mécanique des Fluides, Ecole Militaire Polytechnique, BP 17 Bordj
El-Bahri 16214, Algiers, ALGERIA

b. Arts et Metiers Institute of Technology, CNAM, LIFSE, HESAM University, F-75013
Paris, FRANCE

Abstract :

A passive flow control strategy for four different aerofoils (NACA0012, NACA6415, S809 and S8036) operating at low Reynolds number applications, was investigated in the current work. The effect of installing micro off-surface rod device with various cross-section shapes (circular, triangular, square, pentagonal and hexagonal) in the vicinity of aerofoils leading edge at flow condition $Re_c = 2.5 \times 10^5$ was experimentally and numerically investigated. A common diameter for each given rod was set to be $d/c = 1.34\%$, where c is the aerofoil chord length. The streamwise in-line and the top cross-stream offset dimensionless spacings were the two parameters that have been considered. Their scaling influence on the flow control effectiveness through aerodynamic loads analysis was examined by mean of wind tunnel measurements. Steady RANS calculations with transition sensitive closure turbulence model ($\gamma - \tilde{Re}_{\theta,t}$) were further supplemented to provide more insights about this flow control method. The main results revealed that these off-surface micro-vortex generators are very effective in controlling the flow at post stall regime for all aerofoils. First, the parasite drag for rod-aerofoil system is small at low incidence angles for both NACA6415 and S809 wings compared to S8036. In the other hand, significant enhancement in lift coefficient can be achieved at post stall, accompanying by pronounced decrease in drag coefficient for all configurations. In addition, results indicate that the heavy stall can be effectively delayed for higher angles.

Key words : Passive flow control, Low Reynolds aerofoil, Micro-rod, Transition sensitive model, off-surface vortex generator, Lift enhancement, Drag reduction.

1 Introduction

The aerodynamics of low Reynolds number engineering applications like low pressure compressors and turbines, vertical axis wind turbines, helicopter blades, unmanned aerial vehicles and micro air vehicles have gained deep attention in recent years. The overall performances of these aerofoils operating at such Reynolds number ranged from 10^4 to 10^5 are vigorously tormented by a phenomenon known as Laminar Separation Bubble. This kind of laminar separation is caused by an early peel off of the laminar boundary layer over the curved wing surface subjected to a strong negative pressure gradient. Thus, the most common explanation for such unusual aerodynamic behaviour is related to the presence of the LSB at certain angles of attack which may generate negative effects on the efficiency of these devices like lift and stability reduction, drag, vibration and noise increase. Thus, understanding the flow characteristics at such regimes and designing a control system that may compensate the undesirable impacts on aerodynamic performance are inevitable for a better aerofoil design methodology. Numerous studies have been conducted to predict the aerofoils behaviour working at low Reynolds number [1], [2], [3] and [4]. It was shown that their attitude at such flow conditions is completely different as against high Reynolds number aerodynamic characteristics [5]. As for these many differences, one of the major issues reported in literature was severe effects on wing stall characteristics which are changed to worse compared to high-speed flows [6]. In the other hand, in addition to drag increase and performance degradation the linear tendency of lift characteristics is completely lost at pre-stall regime configuration [7]. As part of substantial study, it has been proposed by many researchers that these sharp differences between the two regimes could be attributed to the appearance of LSB on the aerofoil suction side [8] and [9]. Thereby, some general inferences of high Reynolds number features cannot be applied directly to such low velocity flows [10] and [11]. Naturally, a widespread research interest has attracted the use of novel flow control techniques to improve the aerodynamic performance of aerofoils at low Reynolds flow applications. Based on energy cost, Gad El-Hak [12] has classified the flow control on three main categories happened to be passive, active and reactive methods. As for laminar flow separation control, the simple and cheap passive techniques have gathered large attention. The idea to suppress or reduce LSB size is by promoting the boundary layer early transition via geometry modification for free transition such as leading-edge tubercles [13] or by introducing artificial vortex generator for forced transition like trip wires, roughness tape strips and surface grooves [14], [15], [16] and [17]. Although these traditional methods are efficient for lift enhancement, they are often accompanied by skin drag penalty. In recent years, researchers have attempted to reduce the drag of elongated bluff body by incorporating an off-surface control element close to its leading edge [18]. In their experiment, authors have demonstrated that the cylinder rod performs better than the on-surface devices stated above and led to totally suppress the LSB on the body suction surface. Despite the effectiveness of such small rods to control flow over bluff bodies, the use of such elements with diameter ratio greater than 8% in case of aerofoils will definitely induce extra drag for the whole system. Consequently, recent numerical investigations were attempted to use much smaller cylinder diameter rods for aerofoil flow control. Luo et al. [19] have adopted a strategy of placing micro-cylinder in the vicinity of NACA0012 wing model. The passive control effects on post stall region at high Reynolds and high angles of attack flow conditions were conclusive. It was found that for an optimum rod configuration of d/c ranged [1% – 1.5%] and $L/c = 1.5\%$ a delay of 2° in heavy stall was observed accompa-

nying an important lift enhancement and pronounced drag reduction. Furthermore, Shi et al. [20] and Shi et al. [21] numerically studied the use of typical tiny cylinder off-surface vortex generator to disturb the separated flow on stalled S908 aerofoil at a Reynolds number of 10^6 . The main results showed that the static micro-cylinder was effective to suppress the flow separation hence improve the overall performance of the aerofoil. In addition, for cases where static tiny rod configuration fails to produce any amelioration a better flow control can be achieved with optimal oscillating mode such that a 88% lift to drag ration was attained.

In view of this, most of the above-mentioned studies attempted to investigate numerically the influence of micro-cylinder on flow field over aerofoils at post stall angles and high Reynolds numbers, seeking to provide the flow concepts that are responsible for aerodynamic performance gain. Likewise, the experimental studies that report the control of laminar flow separation over aerofoils at low Reynolds applications are extremely limited and focused on using conventional flow control techniques only. In the current work, the influence of tiny rods of different shapes placed in the vicinity of leading edge on the aerodynamic characteristics over NACA0012, NACA6415, S809 and S8036 wings for both pre and post stall angles at Reynolds number of 2.5×10^5 is experimentally and numerically investigated. Different rod positions have been tested, namely, $1 \times d$, $2 \times d$, $3 \times d$ and $4 \times d$ at various incidence angles. The obtained flow field data for such rod-aerofoil systems at low-speed flow could be handy in understanding the flow mechanisms for an effective engineering design of such applications. Deep aerodynamic performance analysis for each considered case are carried out for both baseline and controlled cases to emphasis the effect of this off-surface vortex generator on aerodynamic performance.

2 Experimental Set Up

2.1 Wind Tunnel

The current tests were conducted in a low-speed, Eiffel-type wind tunnel with a square test section of dimensions $0.6 \text{ m} \times 0.6 \text{ m}$ at Fluid Mechanics Laboratory, EMP School Algeria. In order to reduce boundary layer effects of the test section walls and maintain a constant static pressure, the cross-sectional area of the contraction nozzle was 9 : 1, and its both side walls were enlarged with a divergence angle of 0.3° . A pressure transducer was connected to a Pitot-static tube upstream of the different aerofoil models to measure the freestream velocity of the flow. The freestream turbulence intensity at the centreline was 0.5% at the tunnel maximum speed of 40 m/s , and reaches a value of 0.85% for lower speeds. All experiments were carried out at a chord-based Reynolds number of 2.5×10^5 at a flow velocity of 21 m/s (Fig.1). The TE81 three components force balance was used to measure the lift and drag for each studied case. It is attached directly to the test section of the tunnel and provides an easy-to-use support system for the models and all loads are monitored by TQ DATASLIM software via a computer. The overall uncertainty on each measured force is $\pm 0.2N$. The blockage ratio in this wind tunnel for the tested aerofoils at their respective range of angles of attack was examined and seemed to be less than 6% up to 35° incidence. Therefore, a blockage correction for the drag coefficient is not necessary as when its value is under 10% its effect on the experiments is negligible.

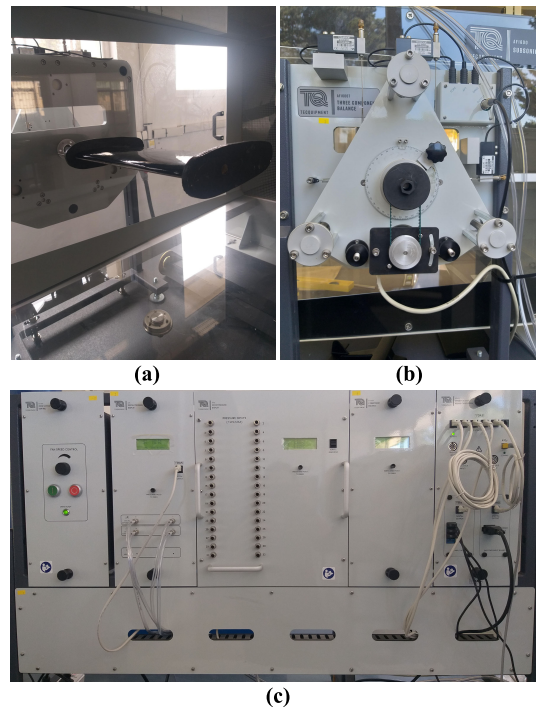


FIGURE 1 – (a) Aerofoil in the wind tunnel test section, (b) TE81 aerodynamic force balance, (c) Standing control cabinet.

2.2 Aerofoil Models

Four aerofoil wing models were manufactured during this study as follow : NACA0012, NACA6415, S809 and S8036. Each model was first designed in a CAD model according to its profile coordinates which is then introduced to a CNC hot-wire cutting machine to prepare the wing from a Polystyrene Foam of high density via DevFoam-3D software developed in the laboratory. After that, a set of glass fibre fabric layers were laid one by one on the foam-based aerofoil shapes and mixed with epoxy resin and the appropriate amount of its hardener (5 : 1 ratio). Later, all aerofoils were left into their respective molds to solidify for about 24 hours at a room temperature to fulfil their curing period and reach the maximum possible strength. Next, both edges of each solid wing model were shaved and a special wood putty was applied on its up and down surfaces and smoothed using a fine sand paper to approximate each profile definition within an accuracy of 0.1 mm . Later all aerofoil models were covered by very fine black sticker using hair-dryer to obtain very smooth surfaces and wooden end plates were assembled to their ends to avoid the side effects. Finally, the manufactured aerofoils have a chord length of 150 mm and a span width of 450 mm (Fig.2). In the other hand, a circular cylindrical rod with a diameter of $d/c = 1.34\%$ was made with a piano-wire material that has a high bending resistance. Then, four tiny rods with triangular, square, pentagonal and hexagonal cross-sections which have common diameter with the micro-cylinder one as shown in figure.3–a were machined from a steel bloc rich in carbon by a method called electro-erosion wire cutting CNC machine which is very precise in cutting such tiny dimensions of the different rods with high precision as it takes about 12 hours to machine one single rod (Fig.3–b).



FIGURE 2 – Manufacturing process of the studied aerofoils.

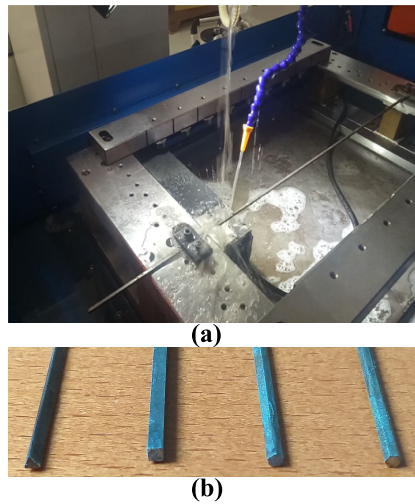


FIGURE 3 – (a) CNC hot-wire cutting machine , (b) Micro-rod shapes.

2.3 Test Case

The use of off-surface micro-vortex generators of various shapes were investigated to control the flow separation over different aerofoil models working at low Reynolds number (Fig.4). It consists of placing tiny rods that have a common diameter, d and different cross section respectively triangular, square, pentagonal and hexagonal form. The efficiency of such passive control technique; different from the conventional ones; is deeply examined throughout the numerical and experimental studies conducted in the current work. The idea behind this strategy involves a mutual interaction between the trailing vortices generated by the different small rods and the suction side boundary layer of the aerofoils subjected to laminar flow separation phenomenon. The rods cross-section dimensions were, $d/c = 1.34\%$ and their gap to the leading edge in the upstream direction was set to the optimal configuration that have the advantage of having a contribution to improving aerodynamic performances when it is applied to NACA0012 aerofoil model [22].

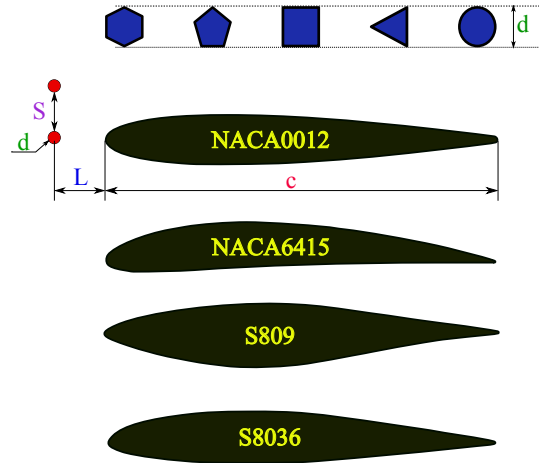


FIGURE 4 – Tested cases with geometric parameters.

3 Computational Methodology

3.1 Computational Domain and Grid

Figure.5 depicts the computational domain adopted in the simulation process. The distance between the inlet boundary to the aerofoil leading edge was set to be $12 \times c$ and extended rearward to 30 times the chord length, which are large enough to guarantee the fully developed flow and avoid any boundary influence on the overall solution. As can be seen, the whole CFD domain was divided into 10 blocks. The aerofoil was enveloped inside a circular block (Block-7) to easily change the angle of attack for different cases. To well capture the flow separation close to the aerofoil walls an O-grid topology was adopted for extremely fine mesh to be used for the boundary layer in the vicinity of the walls such that the y^+ is less than unity. For the remaining domain a C-grid topology was selected in which the cell size increases in all direction starting from the circle and become coarser in Blocks 1, 3, 4 and 9 in order to reduce the calculation cost without losing accuracy (fine mesh close to the model and its wake) due to the coarser mesh in the far regions. In all simulations, the structured mesh was generated using Gambit software. For grid dependence analysis, four different meshes were generated by varying the number of nodes around the aerofoil circumference such that 150, 250, 450 and 650 nodes are chosen. By comparing the aerodynamic coefficients computed from the meshes, no significant variation was seen beyond mesh-3, thus, 450 nodes distribution was considered the most appropriate for the current investigation. The same strategy was adopted with each control device shape, such that 200 nodes around the rod circumference seemed to be large enough to capture all aerodynamic features generated by such small vortex generators.

3.2 Simulation Strategy

The incompressible flow of air described by Navier-Stokes equations was numerically modelled within the framework of general purpose ANSYS-Fluent 18.2 CFD software. Constant material properties for the working fluid were taken into account along with no heat transfer effects. The SIMPLE algorithm was used for velocity-pressure coupling along with a second-order scheme discretization for the pressure terms. Due to the structured topology of the adopted mesh, the least square based method was used to calculate the spatial gradients. To be in line

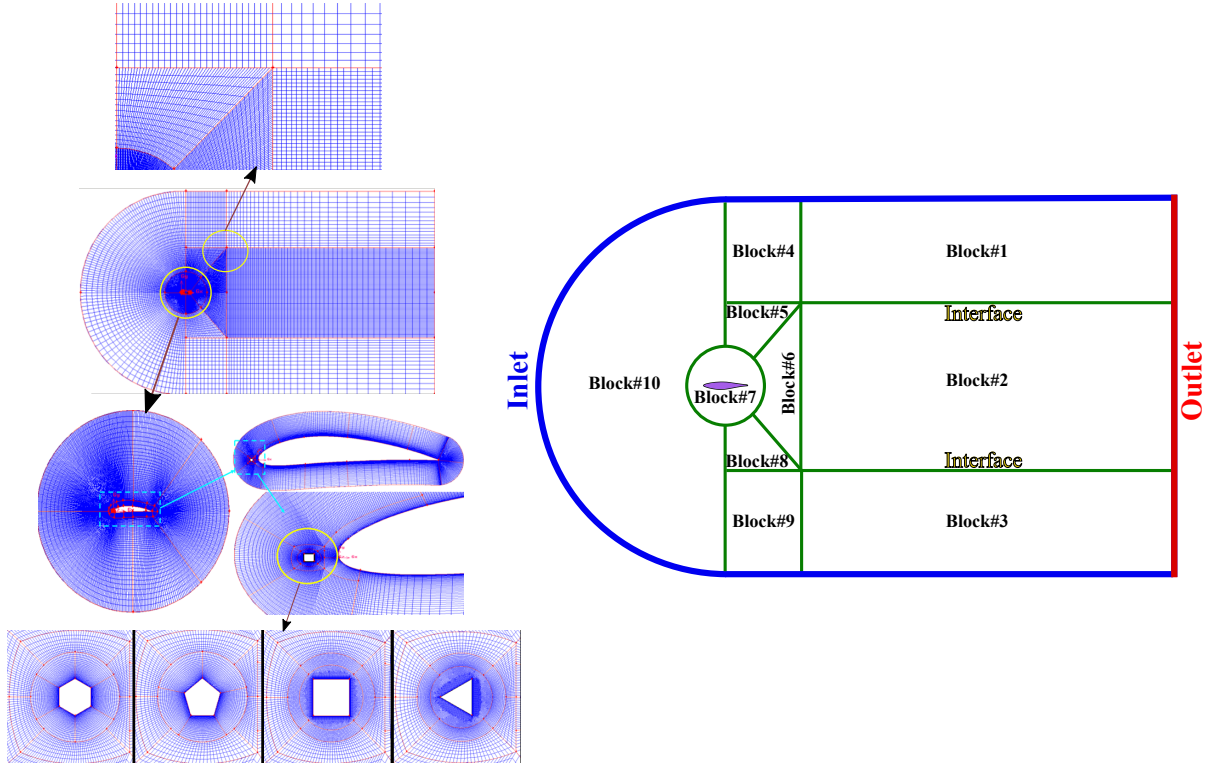


FIGURE 5 – Computational domain and mesh generation.

with the recommended discretization for convective terms given by Lanfrit [23], the second order accurate upwind scheme for all variables was used. Turbulence was modelled by the four equations $\gamma - \tilde{Re}_{\theta,t}$ transition sensitive closure model (Transitional SST) for all simulations. It was shown that this model offered substantial improvements in terms of surface flow patterns, flow separation and aerodynamic loads prediction at low Reynolds number in comparison with classical fully turbulent models ($k - \varepsilon$, $k - \omega$, $k - \omega$ SST, ...), where no laminar effects are included. Its formulation is mainly based on the classical $k - \omega$ SST turbulence model, except two other transport equations for the intermittency (Eq.(1)) is used to handle the triggering of the transition of the boundary layer and the transition momentum thickness based Reynolds number (Eq.(6)). The most important interest that needs to be reported is the need for calibration of the two local correlation parameters Re_{θ_c} and F_{length} reported by Mauro et al. [24] to allow the model to achieve an accurate prediction of flow separation, stall and lift and drag coefficients. Thus, these two parameters can be given by the two Reynolds number based polynomials as shown in equations (4) and (5). For the boundary conditions, a velocity inlet was applied at the upstream boundary according to the considered Reynolds number of 2.5×10^5 and the downstream boundary was set to standard atmospheric pressure, 101.325 kPa and temperature, 288.15 K . The turbulence quantities at the inlet boundary were prescribed as $k = 2.53 \text{ m}^2 \text{ s}^{-2}$, $\omega = 151.55 \text{ s}^{-1}$ and an intermittency factor of, $\gamma = 0.85$. A turbulence intensity of 5% with an integral length scale of 0.15 m were set at the outlet boundary. Finally, all aerofoil surfaces were defined as no-slip wall boundary condition. The flow field was initialized to static pressure, velocity and turbulent quantities prescribed at the inlet boundary. The convergence of the solution was deemed to be achieved at 25000 iterations where all absolute

scaled residuals had decreased below 10^{-7} .

$$\frac{\partial(\rho \gamma)}{\partial t} + \nabla \bullet (\rho U \gamma) = \nabla \bullet \left(\left(\mu + \frac{\mu_t}{\sigma_\gamma} \right) + \nabla \gamma \right) + P_\gamma - D_\gamma \quad (1)$$

$$P_{\gamma,1} = F_{\text{length}} C_{a1} \rho S (\gamma F_{\text{onset}})^{C_a} (1 - C_{e1} \gamma) \quad (2)$$

$$F_{\text{onset}1} = \frac{\text{Re}_\nu}{2.193 \text{Re}_{\theta c}} \quad (3)$$

$$\text{Re}_{\theta c} = 3.9592 \times 10^{-16} \text{Re}^3 - 9.598 \times 10^{-9} \text{Re}^2 + 6.884 \times 10^{-4} \text{Re} + 984.0408 \quad (4)$$

$$F_{\text{length}} = 1.7808 \times 10^{-15} \text{Re}^3 - 2.1514 \times 10^{-9} \text{Re}^2 + 8.132 \times 10^{-4} \text{Re} - 91.2135 \quad (5)$$

$$\frac{\partial(\rho \widetilde{\text{Re}}_{\theta,t})}{\partial t} + \nabla \bullet (\rho U \widetilde{\text{Re}}_{\theta,t}) = \nabla \bullet \left(\left(\mu + \frac{\mu_t}{\sigma_{\theta,t}} \right) + \nabla \widetilde{\text{Re}}_{\theta,t} \right) + P_{\theta,t} \quad (6)$$

$$P_{\theta,t} = 0.03 \frac{\rho^2 U^2}{500 \mu} (\text{Re}_{\theta,t} - \widetilde{\text{Re}}_{\theta,t}) (1 - F_{\theta,t}) \quad (7)$$

3.3 Numerical Validation

To validate the computational method adopted in this work, the outcomes from CFD simulation over baseline NACA0012 aerofoil at a Reynolds number of 2.5×10^5 were compared to the experimental results depicted from literature review. The comparison between CFD, experimental and literature data are shown in Figure.6. Jacobs and Sherman [25], have presented wind tunnel experiments in which flow characteristics over NACA0012 aerofoil is deeply investigated at various Reynolds numbers and wide range angles of attack. The obtained results from numerical approach of the current work are validated against the produced experimental data set. As it is seen, for angles of attack less than 12° , CFD predicted forces are in good agreement with wind tunnel data. The highest recorded error is less than 3.5% for lift coefficient and in the order of 5% in case of drag coefficient at post stall angles. Although the results from simulations under predict and over predict the lift and drag coefficient respectively at high incidences, the overall trends shown through CFD analysis are consistent with those occurring in wind tunnel data.

After validation, the control case was analysed by setting up a micro-cylinder with a diameter of $d/c = 1.34\%$ in the vicinity of the leading edge at a distance, L (Fig.7). The scaling of this gap is done according to the corresponding formation length of the eddies behind the tiny cylinder at the prescribed flow conditions (21 m/s freestream velocity). In accordance with Norberg [26], experimental investigation, for a given Reynolds number happened to be in the order of $3k$ based on the micro cylinder diameter ; the formation length is roughly in the order of $2 \times d$. Thus, four values of L were selected provided that they spread out over a range likewise the off-surface vortex generator laid out before formation, within the formation, after the formation

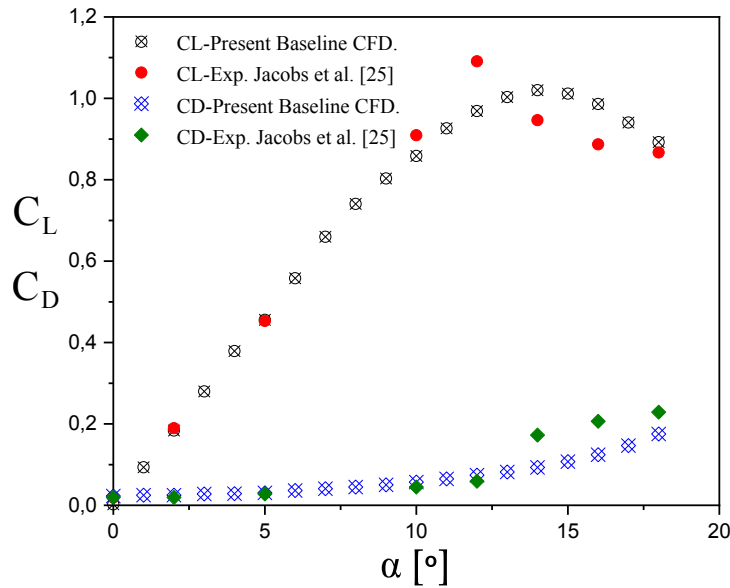


FIGURE 6 – Comparison between the current CFD results and literature experimental data (Test condition : $Re_c = 2.5 \times 10^5$).

and far away from the formation zone. These chosen L values were respectively $1 \times d$, $2 \times d$, $3 \times d$ and $4 \times d$. The sensitivity analysis for L scaling over the maximum lift to drag ratio to the baseline configuration is explicitly depicted in figure.8. The plot shows that the $(C_L/C_D)_{max}$ is very sensitive to the rod position. The benefit changes, in term of $(C_L/C_D)_{max}$, are clearly noticeable for two rod positions, $2 \times d$ and $3 \times d$, where $[(C_L/C_D)_{max}]$ for the first position is 1.04 larger than the baseline ratio and its corresponding value for $3 \times d$ rod location is 1.12. However, a loss in lift to drag ratio for the two other positions, $1 \times d$ and $4 \times d$, is identified, as it seems that the effect of the turbulence generated from these locations are weak and not able to deliver enough energy to the suction side boundary layer which exhibits a degradation in the aerodynamic efficacy of the aerofoil. As a result, after such comprehensive considerations, the experimental analysis of varying the shape of the off-surface tiny control device applied over NACA6415, S809 and S8036 aerofoils at flow condition corresponding to 2.5×10^5 Reynolds number is considered for a non-dimensional spacing of $L/d = 3$ for the reaming experimental investigations.

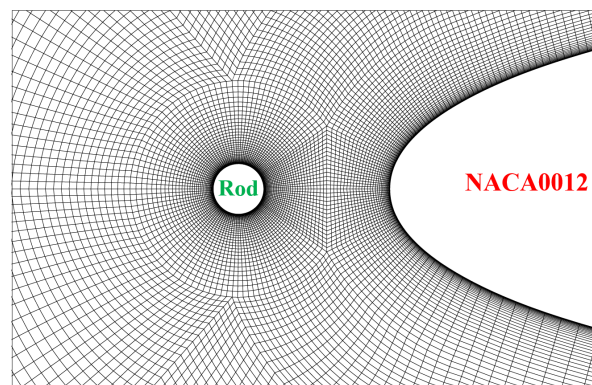


FIGURE 7 – Generated mesh for NACA0012 aerofoil controlled by micro-cylinder rod.

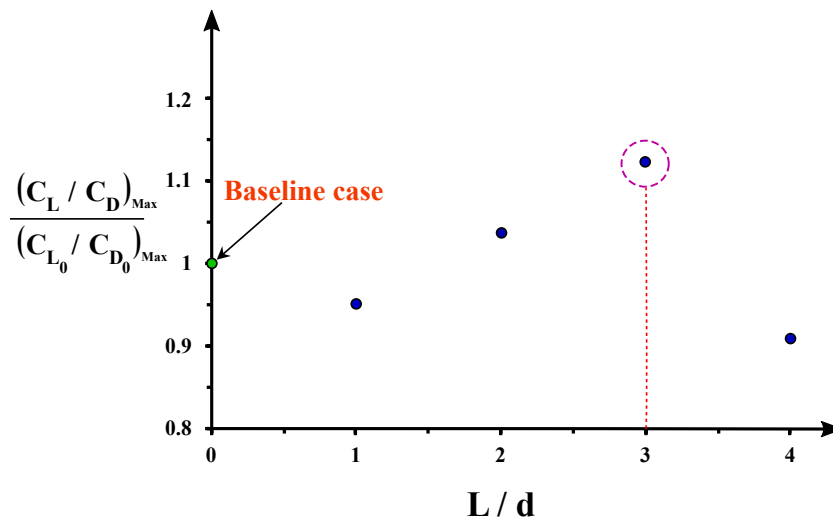


FIGURE 8 – Effect of scaling, L on NACA0012 aerodynamic performance (Test conditions : $Re_c = 2.5 \times 10^5$ and $d/c = 1.34\%$).

4 Results and Discussions

4.1 Experimental Validation

This section describes detailed experimental investigations to analyse the effects of leading-edge rod vortex generator of different cross-section shapes (triangular, square, pentagonal and hexagonal) on the static aerodynamic performance of three different aerofoils NACA6415, S809 and S8036 at a Reynolds number of 2.5×10^5 . All rods have a common diameter of $d/c = 1.34\%$ which is small enough to avoid any vibration parasites over the flow field. The impact of such passive flow control technique on both lift and drag coefficients is comprehensively studied and the optimum location of this tiny device was set at $L/d = 3$ as it was the most processing spacing that brought a gain on the overall aerodynamic efficiency of symmetric aerofoil (NACA0012) as shown previously. First of all, a validation of the wind tunnel measured loads for each baseline aerofoil was considered by a deep comparison on the available data from literature for the same flow conditions. The Pearson correlation between two data set X and Y is given by $r_{X,Y} = \frac{cov(X,Y)}{\sigma_X \times \sigma_Y}$. This coefficient represents a good indicator for the existence and degree of linear relationship between two sets of data, thus using such statistical parameter for data validation seems to be very practical. Figure.9 depicts the variation of both C_L and C_D coefficients over a wide range of angles of attack for the baseline case of all studied aerofoils for the considered flow conditions. All measured forces were substantially compared to the available CFD and experimental data taken from the works presented in references [27, 28, 29, 30, 31]. By applying the Pearson correlation for each pair of data sets, the minimum recorded value for, r was 0.9521 in such a way that any value of this coefficient laying in the range of 0.9 to 1 indicates the existence of a very strong correlation between data sets. Therefore, the present wind tunnel measured lift and drag coefficients agree well with both numerical and experimental results taken from literature especially at pre-stall flow angles. In addition, from the above comparison and validation, it can be clearly seen that the experimental procedure adopted in this current study was capable of reproducing the aerodynamic coefficients of the low Reynolds flow around the different considered aerofoils over wide range of working angles.

4.2 Effect of the Control Technique

Figures 10 and 11 depict the lift and drag coefficients respectively of the three aerofoils considered in this work for the baseline and by applying the passive control technique using the four selected rod shapes. We notice that the rods have an obvious effect on the aerodynamic coefficients of these aerofoils at the current flow conditions. For the optimal rods configuration such that the case with a diameter of 1.34% the chord length and a distance of 3 times its diameter, both lift and drag curves are obviously higher than the original ones especially at large angles of attack. In case of NACA4615, the maximum lift increase was achieved by a triangular rod at post stall regime with relatively 80% improvement at 23°. Whereas, hexagonal rod shape took the lead at post-stall angles with a drag reduction of 13% at 19° incidence. Overall, these aerodynamic enhancements were highly highlighted as a delay of 4° in stall angle was observed. In addition, for S809 wing model, the square rod seemed to be more efficient with 30% pronounced drag drop at 20°. As for lift coefficient the pentagonal rod showed an ability of enhancing it by 13% compared to the other shapes. Furthermore, the effect of the square rod on the performances of S8036 were more promising than other forms as it was able to improve the lift significantly by 70% and reduce the drag by 15% in comparison to remaining rod, accompanying an effective delay of heavy stall by 7°. So to sum up, the effectiveness of the rods on the lift coefficient is declined at low angles of attack, whereas, the effectiveness trend is reversed at post stall regime for all aerofoils. Moreover, in comparison with baseline cases, lift-to-drag ratio was improved for all rod-aerofoil configurations, as well as the pronounced delay in stall angle. Thus, the adopted control elements are beneficial for improving the overall aerodynamic performance of the studied aerofoils.

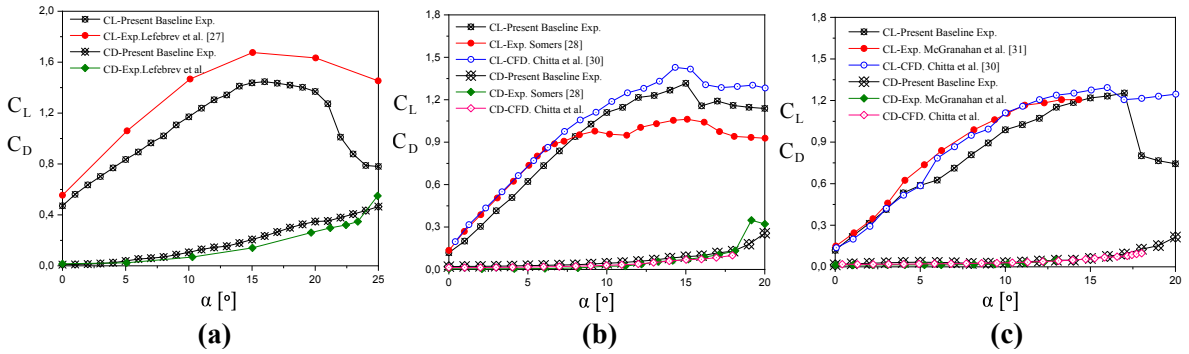


FIGURE 9 – Experimental validation of lift and drag coefficients (Test conditions : $Re_c = 2.5 \times 10^5$, $d/c = 1.34\%$ and $L/d = 3 \times d$), (a) for NACA6415 model, (b) for S809 model, (c) for S8036 model.

5 Conclusion

In this work, detailed experimental and numerical analysis were performed to assess the effect of setting small off-surface vortex generators near the leading edge of various aerofoils (NACA0012, NACA6415, S809 and S8030) over their aerodynamic performances. Some useful conclusions can be drawn as follows : The spacing between the small device and the leading edge of a given NACA0012 aerofoil has appreciable effects on lift to drag ratio force, thus a gap of 3 times

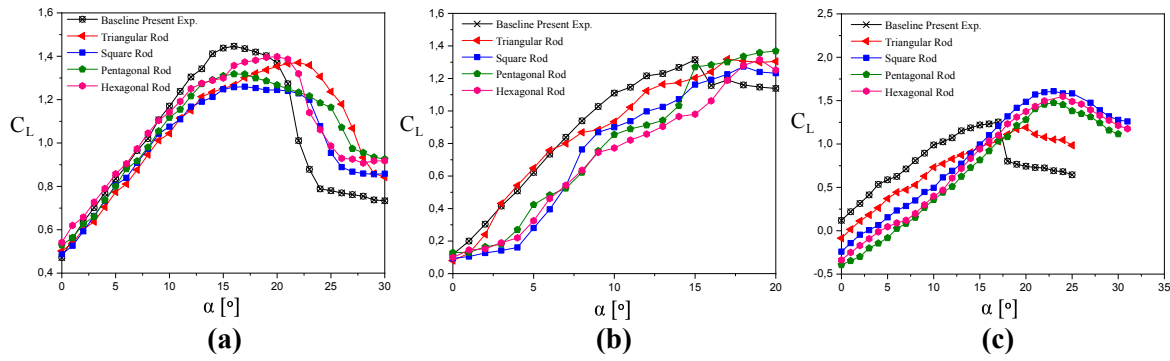


FIGURE 10 – Effect of the off-surface vortex generator shapes on lift coefficient, (Test conditions : $Re_c = 2.5 \times 10^5$, $d/c = 1.34\%$ and $L/d = 3 \times d$), (a) for NACA6415 model, (b) for S809 model, (c) for S8036 model.

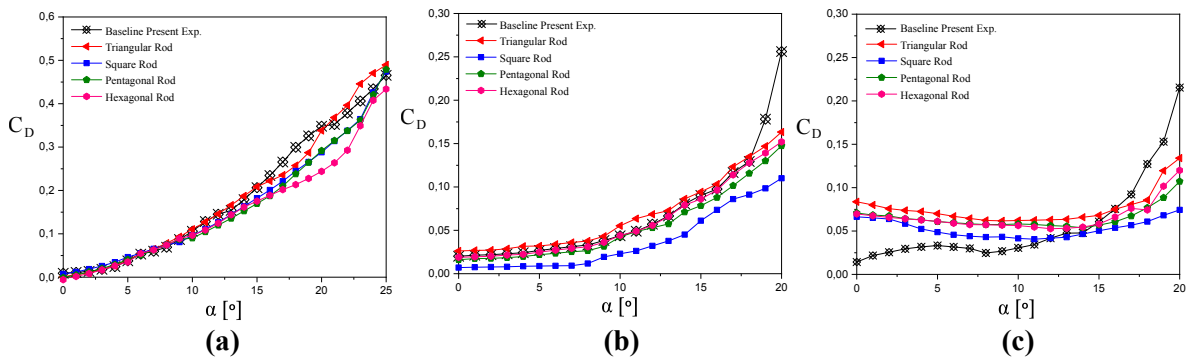


FIGURE 11 – Effect of the off-surface vortex generator shapes on drag coefficient (Test conditions : $Re_c = 2.5 \times 10^5$, $d/c = 1.34\%$ and $L/d = 3 \times d$), (a) for NACA6415 model, (b) for S809 model, (c) for S8036 model.

the rod diameter was considered for rod shapes analysis. Furthermore, for aerofoils working at post stall regime, the leading-edge rod can effectively enhance the aerodynamic performance over significant extent and delay the stall angle. The maximum lift increase was achieved by a triangular rod at post stall regime with relatively 80% improvement and the square rod seemed to be more efficient with 30% pronounced drag drop accompanying an effective delay of heavy stall by 7°. Furthermore, in case of NACA4615, the maximum lift increase was achieved by a triangular rod at post stall regime with relatively 80% improvement at 23°. Whereas, hexagonal rod shape took the lead at post-stall angles with a drag reduction of 13% at 19° incidence. Overall, these aerodynamic enhancements were highly highlighted as a delay of 4° in stall angle was observed. In addition, for S809 wing model, the square rod seemed to be more efficient with 30% pronounced drag drop at 20°. As for lift coefficient the pentagonal rod showed an ability of enhancing it by 13% compared to the other shapes. Furthermore, the effect of the square rod on the performances of S8036 were more promising than other forms as it was able to improve the lift significantly by 70% and reduce the drag by 15% in comparison to remaining rod, accompanying an effective delay of heavy stall by 7°. Finally, the physical analysis of flow field controlled by the rods around these aerofoils obtained by CFD simulations at most relevant configurations had illustrated the flow structure mechanisms of the control elements in aerofoils' aerodynamic improvements.

Références

- [1] Hu, H. ; Yang, Z. : An Experimental Study of the Laminar Flow Separation on a Low-Reynolds-Number Airfoil. *Journal of Fluids Engineering*, Vol. 130, No. 3, pp. 283–309, 2008.
- [2] Genc, M.S. ; Karasu, I. ; Acikel, H.H. : An experimental study on aerodynamics of NACA2415 aerofoil at low Re numbers. *Experimental Thermal and Fluid Science*, Vol. 39, No. 1, pp. 252–264, 2012.
- [3] Choudhry, A. ; Arjomandi, M. ; Kelso, R. : A study of long separation bubble on thick airfoils and its consequent effects. *International Journal of Heat and Fluid Flow*, Vol. 52, No. 1, pp. 84–96, 2015.
- [4] Somashekar, V. ; Raj, A.I.S. : Experimental Investigation on Laminar Separation Bubble Over an Airfoil – A Review. *Indian Journal of Science and Technology*, Vol. 11, No. 11, pp. 1–9, 2018.
- [5] ElJack, E. : High Fidelity Numerical Simulation of the Flow Field around NACA0012 Aerofoil from Laminar Separation Bubble to a Full Stall. *International Journal of Computational Fluid Dynamics*, Vol. 31, No. 4–5, pp. 230–245, 2017.
- [6] Winslow, J. ; Otsuka, H. ; Govindarajan, B. ; Chopra, I. : Basic Understanding of Airfoil Characteristics at Low Reynolds Numbers ($10^4 - 10^5$). *Journal of Aircraft*, Vol. 55, No. 3, pp. 1050–1061, 2018.
- [7] Aguilar-Cabello, J. ; Gutierrez-Castillo, P. ; Parras, L. ; Del-Pino, C. ; Sanmiguel-Rojas, E. : On the Onset of Negative Lift in a Symmetric Airfoil at very Small Angles of Attack. *Physics of Fluids*, Vol. 32, No. 5, pp. 055107, 2020.
- [8] ElAwad, Y.A. ; ElJack, E.M. : Numerical Investigation of the Low-Frequency Flow Oscillation over a NACA0012 Aerofoil at the Inception of Stall. *International Journal of Micro Air Vehicles*, Vol. 11, No. 1, pp. 1–17, 2019.
- [9] ElJack, E. ; Soria, J. ; ElAwad, Y. ; Ohtake, T. : Simulation and Characterization of the Laminar Separation Bubble over a NACA0012 Airfoil as a Function of Angle of Attack. *Physical Review Fluids*, Vol. 6, No. 3, pp. 034701, 2021.
- [10] Ohtake, T. ; Sakai, Y. : Characteristics of Unsteady Flow Field of Laminar Separation Bubble on a Naca0012 Airfoil at Low Reynolds Numbers. *18th International Symposium on Flow Visualization Zurich, Switzerland, June 26-29, ETH Zurich, 2018.*
- [11] Masayuki, A. ; Daiki, H. : High Performance Airfoil with Low Reynolds Number Dependence on Aerodynamic Characteristics. *Fluid Mechanics Research International Journal*, Vol. 3, No. 2, pp. 76–80, 2019.
- [12] Gad-El-Hak, M. : *Flow Control : Passive, Active, and Reactive Flow Management*. Cambridge University Press, 2000.
- [13] Sudhakar, S. ; Karthikeyan, N. ; Suriyanarayanan, P. : Experimental Studies on the Effect of Leading-Edge Tubercles on Laminar Separation Bubble. *AIAA Journal*, Vol. 57, No. 12, pp. 5197–5207, 2019.
- [14] Manolesos, M. ; Voutsinas, S.G. : Experimental investigation of the flow past passive vortex generators on an airfoil experiencing three-dimensional separation. *Journal of Wind Engineering and Industrial Aerodynamics*, Vol. 142, No. 1, pp. 130–148, 2015.

- [15] Wang, H. ; Zhang, B. ; Qiu, Q. ; Xu, X. : Flow control on the NREL S809 wind turbine airfoil using vortex generators. *Energy*, Vol. 118, No. 1, pp. 1210–1221, 2017.
- [16] Bull, S. ; Chiereghin, N. ; Cleaver, D.J. ; Gursul, I. : A novel Approach to Leading Edge Vortex Suppression. *AIAA Journal*, Vol. 58, No. 11, pp. 4212–4227, 2020.
- [17] Yadav, R. ; Bodavula, A. : Numerical Investigation of the Effect of Triangular Cavity on the Unsteady Aerodynamics of NACA0012 at a Low Reynolds Number. *Proceedings of the Institution of Mechanical Engineers, Part G : Journal of Aerospace Engineering*, Vol. 236, No. 6, pp. 1064–1080, 2022.
- [18] Michelis, T. ; Kotsonis, M. : Interaction of an off-surface cylinder with separated flow from a bluff body leading edge. *Experimental Thermal and Fluid Science*, Vol. 63, No. 1, pp. 91–105, 2015.
- [19] Luo, D. ; Huang, D. : Passive flow control of a stalled airfoil using a microcylinder. *Journal of Wind Engineering and Industrial Aerodynamics*, Vol. 170, No. 1, pp. 256–273, 2017.
- [20] Shi, X. ; Xu, S. ; Ding, L. ; Huang, D. : Passive flow control of a stalled airfoil using an oscillating micro-cylinder. *Computers and Fluids*, Vol. 178, No. 1, pp. 152–165, 2019.
- [21] Shi, X. ; Sun, J. ; Zhong, S. ; Huang, D. : Flow Control of a Stalled S809 Airfoil using an Oscillating Micro-Cylinder at Different Angles of Attack. *Renewable Energy*, Vol. 175, No. 1, pp. 405–414, 2021.
- [22] Larabi, A. ; Pereira, M. ; Ravelet, F. ; Azzam, T. ; Oualli, H. ; Menfoukh, L. and Bakir, F. : Numerical Study on the Effect of an Off-Surface Micro-Rod Vortex Generator Placed Upstream NACA0012 Aerofoil. *EDP Sciences E3S Web of Conferences*, Vol. 321, No. 1, pp. 01011, 2021.
- [23] Lanfrit, M. : Best practice guidelines for handling Automotive External Aerodynamics with FLUENT. southampton.ac.uk, Corpus ID : 165159674, 2005.
- [24] Mauro, S. ; Lanzafame, R. and Messina, M. : Transition turbulence model calibration for wind turbine airfoil characterization through the use of a micro-genetic algorithm. *International Journal of Energy Environment Engineering*, Vol. 8, pp. 359–374, 2017.
- [25] Jacobs, E. N. and Sherman, A. : Airfoil section characteristics as affected by variations of the Reynolds number. *NACA Technical Report*, Vol. 586, No. 1, pp. 227–267, 1937.
- [26] Norberg, C. : LDV-Measurements in the Near Wake of a Circular Cylinder. *Proceedings of the Conference on Bluff Body Wakes and Vortex Induced Vibration*, Washington DC, Edited by P.W. Bearman and C.H.K. Williamson (Cornell University, Ithaca, NY), pp. 1–12, 1998.
- [27] Lefebvre, A. ; Dano, B. ; Bartow, W. B. ; Difronzo, M. and Zha, G. : Performance and energy expenditure of coflow jet airfoil with variation of mach number. *Journal of Aircraft*, Vol. 53, No. 6, pp. 1757–1767, 2016.
- [28] Somers, D. M. : Design and experimental results for the S809 airfoil. *National Renewable Energy Lab.(NREL)*, Golden, CO (United States), NREL/SR-440-6918, 1997.
- [29] Gomes, A. O. ; Brito, R. F. ; Rosa, H. M. P. ; Campos, J. C. C. ; Tibiriça, A. M. B. and Treto, P. C. : Experimental analysis of an S809 airfoil. *Revista de Engenharia Térmica*, Vol. 13, No. 2, pp. 28–32, 2014.

- [30] Chitta, V. ;Jamal, T. and Walters, D. K. : Numerical investigation of low-Reynolds number airfoil flows using transition-sensitive and fully turbulent RANS models. Proceedings of the ASME 4th Joint US-European Fluids Engineering Division Summer Meeting August 3–7, 2014, Chicago, Illinois, USA, Vol. 46247, pp. V01DT27A012, 2014.
- [31] McGranahan, B. and Selig, M. : Surface oil flow measurements on several airfoils at low Reynolds numbers. 21st AIAA applied aerodynamics conference, pp. 4067, 2003.